Omega-P, Inc.
199 Whitney Ave., Suite 200, New Haven, CT 06511

HIGH-POWER Ka-BAND WINDOW AND RESONANT RING

FINAL TECHNICAL REPORT

Phase I SBIR Grant #DE-FG02-05ER 84395

TABLE OF CONTENTS

Principal Investigator: J. L. Hirshfield
jay@omega-p.com

November, 2006

I. INTRODUCTION

Under Topic 37b in the DoE 2005 SBIR Program Solicitation, the following is stated: "Upgrades to the next generation linear collider will require many RF power handling components which are not presently available, e.g., RF windows, couplers, mode transformers, rf loads, and high-power rings capable of operating at high powers (10-100 MW), high frequencies (1-40 GHz), and pulse lengths of several microseconds. Therefore grant applications are sought for passive and active RF components such as over-moded mode converters from rectangular to circular waveguide, high-power RF windows, circulators, isolators, switches, and quasi-optical components." Omega-P, Inc. submitted a proposal entitled "High-Power Ka-Band Window and Resonant Ring" in response, and was awarded the Phase I grant DE-FG02-05 ER 84368, with the same title. The goal of the project was to develop high-power RF windows to operate at a frequency within the range 30-35 GHz. In addition, for testing these windows (or any other low-insertion-loss component) to the level of 100's of MW where accelerator applications are foreseen, a high-gain resonant ring was also to be (further) developed within the same project. As will be shown below, both the window and the resonant ring incorporate over-moded mode converters and mode transformers, so the design techniques to be perfected and tested during this project can be applied as well for use in developing other required high-power over-moded components.

The need for experimental facilities for basic investigations leading to research and development of new high-gradient accelerator technology has intensified recently, as the accelerator community has come to accept the need for fundamental studies of processes that limit RF fields in room temperature ("warm") structures. On March 3, 2006 Dr. Robin Staffin, Associate Director, Office of High Energy Physics DoE, testified to HEPAP regarding the FY2007 HEP budget on the request for

> "…significant increase….in the long-range R&D program that supports fundamental research into the physics of….'accelerator science.' The goal is to enable the restoration of the accelerator science research program to the level needed to support long-term R&D on new particle acceleration techniques and technologies, such as novel particle acceleration concepts, very high gradient accelerating structures, and user facilities to test these concepts…."

The Omega-P project described in this report is for development of key technological components needed for production of the high power RF pulses required to carry out experiments referred to by Dr. Staffin. These key components include a high-power barrier window capable of efficient transmission of Ka-band RF power levels up to 200 MW, and a resonant ring to produce effective (circulating) power levels at high multiple levels of the power directly available from an RF source, for testing of the window and other components. These components are essential for anticipated use of the 100-200 MW, 50-70 ns Ka-band pulses needed to carry out fundamental experiments on RF breakdown, and to expose candidate accelerator structures to RF surface electric fields of many 100's of MV/m. These 100-200 MW pulses are to be produced using 20-40 MW, 1 μs pulses from the Yale/Omega-P 34.3 GHz magnicon that are to be compressed in active and passive pulse compressors now under development, under other Phase II SBIR grants from DoE to Omega-P. But before those high-power compressed pulses can be transmitted to experimental test structures, a barrier window must be developed and tested. That window development is at the core of this project.

Development of the barrier window and resonant ring are encouraged by test results of the 34.3 GHz third-harmonic magnicon amplifier [1] developed by Omega-P, and now operating at Yale. The magnicon has a design power of over 40 MW in 1 μsec pulses. The fully assembled tube is shown in Fig. 1. RF conditioning continues, but the magnicon already produces an output power of over 30 MW in stable 0.5 μs pulses, with a gain of 54 dB. Fig. 2 shows a sample output waveform. Slotted line measurements confirm that the output is monochromatic to within a margin of at least 30 dB. No evident obstacle to eventual operation at the full design output has emerged. But these preliminary results already constitute record values for a millimeter-wave accelerator-class amplifier. Preparation is underway for installation of output windows, transmission lines, and a power combiner to enable the full output power to be fed to test structures and to the actively-switched pulse compressor described in this report.

Figure 1. A general view of the 34.3 GHz magnicon.

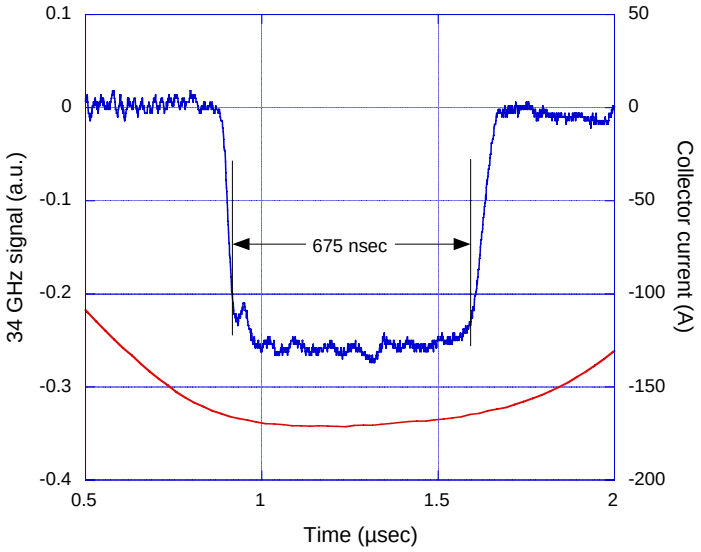

Figure 2. Sample RF output waveform from the 34-GHz magnicon (blue) and magnicon beam current (red).

The overall context for the R&D program outlined here is to enable development of structures and components for the CERN two-beam multi-TeV collider CLIC [2], or a similar future millimeter-wave collider. Tests of CLIC structures require 190 MW of 30-GHz power in 60 ns pulses to drive each 30-cm long accelerating structure to a nominal loaded accelerating gradient of 150 MV/m. For this, the CLIC study team has expressed its need for a stand-alone Ka-band RF test stand to provide this power [3]. Omega-P believes that it can develop a 34-GHz counterpart for this source, by at first employing passive and later active pulse compression, with a power gain of up to 7:1, of 1-μs wide output pulses from its 45-MW, 34-GHz magnion amplifier. But transmission of this intense peak power pulse from the rf source to an accelerator structure under test will require a reliable barrier window, development of which is proposed here. Furthermore, tests of this window to determine its power limits will require a high-gain resonant ring, which can create field strengths at the window corresponding to power levels of several 100's of MW, exceeding levels expected from the active pulse compressor. Development of a resonant ring started during 2002, with successful DoE-sponsored SBIR Phase I design and low-power tests on a non-vacuum prototype showing a power gain of 35:1 [4]; Phase II construction of a high-power version was not approved by DoE in 2004.

Omega-P's development of millimeter-wave technology for accelerator applications is continuing at 34.272 GHz, the operating frequency for its 45-MW magnicon amplifier. DoE-sponsored Phase II SBIR programs on development of high-power components and of a quasi-optical RF pulse compressor at this frequency are currently underway, and the Phase I project on the resonant ring was completed in 2003. The four barrier windows for the four outputs of the magnicon that were built under this program are not designed to operate at power levels high enough to handle singly the magnicon's full 45-MW output, not to mention the higher 200 MW pulses required for structure testing. Omega-P desires to transfer the rapidly-emerging proven 34-GHz technology to 30 GHz to support needs as defined by the CLIC study team. But, so far, what is missing in this program is development of a barrier window capable of

transmitting from the pulse compressor the ~200 MW peak power pulses required for development and test of candidate CLIC structures. The results described here are directed towards remedying that omission, and to provide as well for the resonant ring necessary for high-power test of the window. Although initial development and tests of the window and resonant ring are to be at 34.3 GHz, their designs can be later easily scaled to 30 GHz.

II. TECHNICAL APPROACH FOR PHASE I R&D

Separate descriptions will be given for the technical approaches taken for the barrier window, and for the resonant ring. It will become clear how the ring would be used for high-power tests of the window, as the discussion develops. Other relevant components that have been developed by Omega-P will also be described.

IIa. Barrier Window

A barrier window for accelerator applications is to provide separation between segments of the RF transmission system, such as between an RF source and a load. The window will invariably operate with vacuum on both sides, although it must be built to withstand atmospheric pressure forces during transport and installation of components or test structures. The window should introduce minimal reflections and loss at its design frequency, and not be subject to multipactor discharges on its surfaces within its operating power range. When operation at high average power levels is anticipated, the window design must embody sufficient cooling to avoid overheating and subsequent failure; this is a major challenge for windows used in MW-CW millimeter-wave gyrotrons for plasma heating applications, but is not so severe at the 5-50 kW average power levels that are typical for accelerator systems. The following general principles will be used in the window design:

1. The oversized window disk itself will be made of alumina ceramic (Al_2O_3). Alumina disks are available in quite a large sizes, and the technology is established for brazing such disks with diameters up 100 mm to copper cuffs. Alumina has low microwave losses at 30-35 GHz, with a loss tangent of about $\cdot 10^{-4}$ [5, 8]. The material has reasonable electrical breakdown strength, being able to withstand 4-6 kV/mm electric field (in the indicated frequency range) along the surface for microsecond-length pulses. There exists a long history of using alumina for barrier windows (see e.g 5-7, 9, 10]).
2. The traveling-wave mode of propagation will be used in the dielectric window (see e.g [5, 6]). This, as opposed to the standing-wave mode, allows a significant drop in electric field on the disk surface for a fixed power level, proportional to $\varepsilon^{-1/4}$, where ε is the dielectric permittivity. This drop arises because of disk matching by means of additional reflector elements in the metal waveguide. Since the permittivity for alumina is rather high ε = 9.4-9.7, this can be a valuable advantage.
3. A combination of only TE_{0n} modes will be used, because of their low Ohmic wall attenuation and because of their zero electric fields at the waveguide walls. The latter fact is also important for the window design because in this case the electric field in the most critical window dielectric-metal braze area will be low.

4. A new synthesis technique [11] will be used to design short waveguide transitions to the large window aperture, and to provide an optimal TE_{0n} mode mixture which has a flattened field pattern at the disk. Note that the oversized waveguide cross-section near the disk is highly overmoded: for the preliminary example described here, seven TE_{0n} modes can propagate in the waveguide. It is thus important to design with care the tapers between the input/output waveguides and window apertures. The tapers should have the shortest possible length in order to provide an acceptable frequency band, and should also form an optimal mode mixture with π and 2π mutual phases.

These principles allow one to design a ~200 MW Ka-band window, a preliminary version of which is depicted in Figure 3.

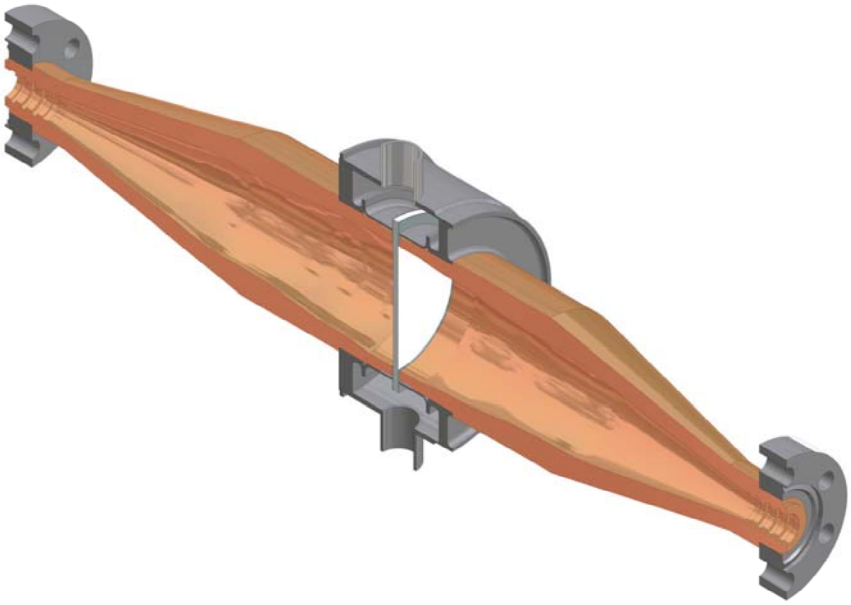

Figure 3. Configuration of proposed barrier window. Shown are mode-mixing up- and down-tapers to the ~63-mm diameter alumina window from 15-mm diameter TE_{01} mode circular waveguide, grooved matching elements at entry and exit to the tapers, and a rigid supporting plenum that provides pump-out access to both sides of the window through holes not shown in the drawing.

IIb. Resonant Ring

A Ka-band resonant ring using a traveling TE_{01} wave in cylindrical waveguide has had preliminary design, fabrication, and low-power tests by Omega-P, under DoE-sponsored SBIR Phase I grant DE-FG02-03ER 83737, entitled *Ka-band resonant ring for high-power testing,* that ran between 07/21/03 and 04/20/04. This project did not win approval for continuation into Phase II, where construction of a high-vacuum, high-power version of the resonant ring would have occurred. That work continued under the project reported here, primarily for testing the barrier window. However, improvements will be incorporated to decrease the losses in the ring, and thus to increase the effective power gain and utility for testing other low-insertion-loss components. Low power measurements have already shown a maximum

effective power gain that exceeded 35:1 at the design frequency of 34.272 GHz. Total quality factor was about 21,400, and the reflection coefficient from the input to the ring resonator was less than 1%. A schematic of the ring is shown in Figure 4.

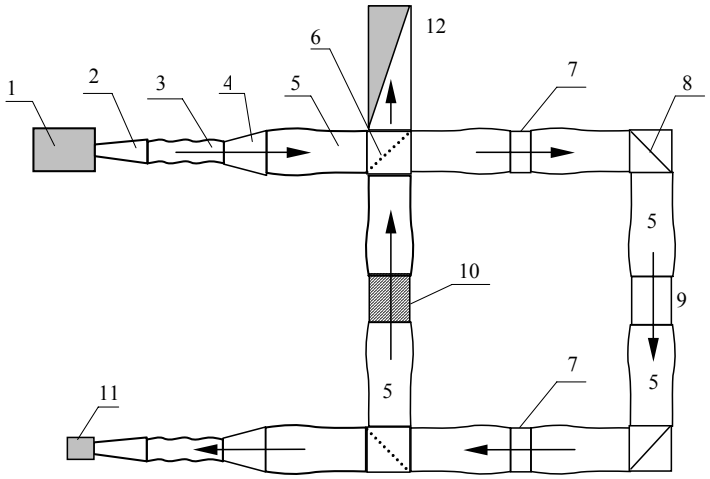

Figure 4. Schematic of overmoded Ka-band high-power resonant ring.

1 – microwave source;
2 – $TE_{10} \Rightarrow TE_{11}$ mode converter;
3 – $TE_{11} \Rightarrow TE_{01}$ mode converter;
4 – TE_{01} waveguide up-taper;
5–$TE_{01} \Rightarrow TE_{01} + TE_{02}$ mode converters;
6 – coupling mirror;
7 – bellows for frequency adjustment;
8 – flat mirror miter bends;
9 – TE_{01} circular waveguide;
10 – component under test;
11 – microwave detector,
12 - microwave load.

The operating mode of the ring is the TE_{01} mode in an oversized circular waveguide. This mode has zero electric field at the waveguide walls and very low Ohmic losses. This mode is a natural choice for the transmission line to feed mm-wave accelerator structures. Furthermore, the proposed barrier window design is based on the use of this mode. Recently a low-loss miter bend operating with this mode was developed. Experimental tests described below show the total loss in the miter bend to be about 1%, including Ohmic and diffraction losses. The resonant ring consists of a directional coupler and straight waveguide runs joined by four miter bends, the latter equipped with vacuum pumping ports. For adjusting the resonant frequency of the ring to be equal to the magnicon operating frequency, a bellows-type adjustable waveguide section is used. The *Q*-factor of the resonator should be about 30,000, a value well within the anticipated frequency stability range of the magnicon. This value of *Q*-factor means that the resonator fill time will be several 10's of ns, a value that is much shorter than the μsec-wide magnicon output pulse. A component under test (i.e., barrier window) would be inserted at position #10, with a straight pipe to extend the length of the opposing arm at #9.

Estimated round trip losses in the ring are approximately 3% including Ohmic losses and losses due to scattering of the operating mode TE_{01} into other modes. Of course, if the component under test that is inserted into the ring has losses of its own, this will reduce the

effective power gain. Figure 5 shows how the gain drops with added loss, for a ring with 35:1 intrinsic gain. Two curves are shown, the lower curve for the case of no change in the ring's coupling constant; the higher curve for change in coupling constant to maximize the gain at each point.

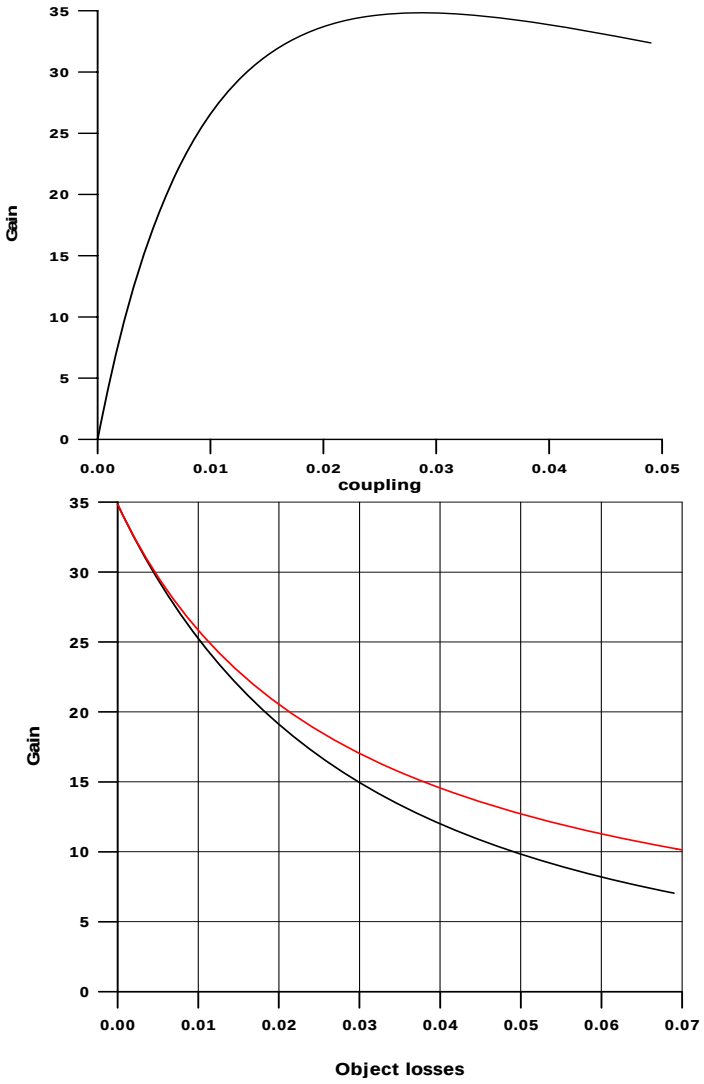

Figure 5. (a) Measured gain power gain in the ring versus coupling; and
(b) reduction in effective power gain due to insertion in the resonant ring of a test component with the level of loss as indicated (b).

For the lower curve (no change in coupling), it is seen that insertion of a component with loss of 3% would reduce the gain to 15:1. If 30 MW power from the magnicon were available (making allowance for transmission losses), this would amount to an effective power level of 450 MW, more than twice that required for a source to test CLIC structures and components, for example.

III. ANTICIPATED PUBLIC BENEFITS

Advancement in high-energy physics has, in the years since WWII, brought enormous practical benefit to the US public in general, and to the US scientific community in particular. Widely-dispersed benefits include fast integrated-circuit electronics, accelerators for radiotherapy and industrial processing, nuclear power, and the internet. For the scientific community, achievements include many discoveries on the fundamental nature of matter and on the origin of the universe. But vexing questions persist, including the nature of dark matter, the origin of mass, extra dimensions, and need "…to illuminate the pathway to the underlying simplicity of the universe.*" Efforts have been carried out by large international research groups that include many scientists trained in the US, using facilities built and operated in the US, thus evincing great pride and prestige among Americans. This positive climate attracted many of brightest young Americans and foreign scholars to high-energy physics and created a scientific work force in the US that is envied and emulated by advanced societies the world over. The curtain on this era in the US could be falling as other countries may be taking the lead in high-energy physics, including the European Community that is now building LHC at CERN in Geneva (with partial US support, it should be said). The international high-energy physics community has pronounced a TeV-scale lepton collider ILC as the next step in its search for a fundamental understanding of Nature. In August 2004, ICFA recommended that, for ILC, a superconducting collider should be built at an initial c-o-m energy of 0.5 TeV, with a possible future upgrade to 0.8 TeV. The competing US/Japan design NLC/GLC that came in behind the superconducting option, in ICFA's view, embodies a room-temperature pair of 10-km microwave-driven linacs, that would be designed to also reach a c-o-m energy of 0.5 TeV, but with possible future upgrade to 1.5 TeV.

So how will the physicist's irrepressible motivation—along with the public's inevitable curiosity—to understand Nature at energies well above 0.8 TeV be satisfied? Room-temperature RF accelerator structures have been proven capable of sustaining an acceleration gradient at least double the 25-35 MeV/m planned for the superconducting linacs in ILC, with—some believe—the potential for much greater values; this could permit construction of a future multi-TeV collider within the geographical footprint anticipated for ILC. Yet issues such as RF breakdown and surface fatigue impose limits and design challenges that must be understood and overcome before a viable plan for a future multi-TeV collider can be formulated. This understanding requires advanced microwave experiments with very high peak powers that can only be achieved through the use of power enhancing RF circuits, including circuits that embody active elements. An essential component that is needed if such high-peak-power tests are to be carried out is a barrier window to separate the RF source (magnicon, power combiner, pulse compressor) from the load under test. For peak power levels at Ka-band of 200 MW or greater no such window exists; thus it is essential that development of a window such as that described here move ahead; otherwise, no high-power testing to make further progress in high-gradient R&D can occur. The resonant ring is needed firstly to test the barrier window, but also to test other high-transmission high-power Ka-band components used in accelerator R&D. These efforts represent important aspects towards enabling tests to be made of candidate accelerator structures at power levels unavailable otherwise, to bring closer to realization a practical multi-TeV collider.

*R. L. Orbach, in oral testimony before the US House Committee on Appropriations, 3/15/05.

IV. RESULTS OF PHASE I R&D

IVa. Technical Objectives of Phase I

The goal of the proposed work was to develop and test a barrier window capable of transmitting Ka-band microwaves in pulses up to 140 ns width, with a peak power level up to 200 MW, and an average power of 5 kW. The technical approach to be taken will follow the general outlines given in Section I. It was planned during Phase I to fabricate and test a prototype of the window at low power, and to prepare high power tests using the 45-MW, 34-GHz magnicon developed by Omega-P. To allow tests during Phase II at effective power levels to 200 MW and beyond, a resonant ring is to be built, having a loaded power gain factor of at least 10:1.

The main goals of the Phase I project were to:

- design a barrier window which is capable to transmit microwave power up to 200 MW in sub-microsecond pulses;
- manufacture a prototype of the window and measure its parameters (transmission, reflection and absorption coefficients) at low power; and
- design the resonant ring with an effective (unloaded) power gain factor of at least 30:1 for the window test at high power with the magnicon.

All the components would be developed for operation at 34.272 GHz frequency, but the designs will be made with a view towards future scaling to 30 GHz.

Results of work on the window and ring design will be described below.

IVb. Study of the multi-mode traveling-wave window

The proposed traveling–wave window is based on a multi-mode wave guide, so all dimensions of the component are many times greater than wavelength. Propagation of many modes results in more difficulties in the window design, but also gives some advantages. To understand clearly the multi-mode traveling –wave window features and to choose properly the window parameters we began the study from a simplified model, then accurate calculations were made by means of scattering matrix code , and then a window mock-up was designed, fabricated and tested. All these stages of the window development will be described below.

IVb.1. Analysis of a simplified model

The basic principles of the traveling wave (TW) window operation could be demonstrated at a simple plane wave model (Fig. 6). The TW-window contains a dielectric slab (of thickness L_d, and permittivity ε) and two reflectors placed at the distances $L_{1,2}$ from the slab. The reflectors are not detailed here and characterized by an amplitude reflection and transmission coefficients, r and t respectively.

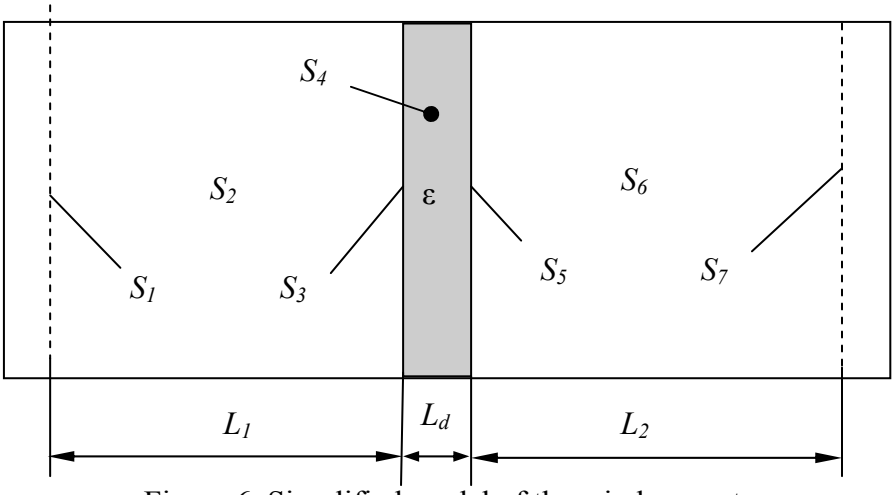

Figure 6. Simplified model of the window system

In this description forward and backward traveling waves have complex amplitudes *F* and *B* correspondingly. Scattering matrix formalism is very useful for the analysis of the window [16]. Each element of the system characterized by the 2×2 scattering matrix, where the diagonal elements are the reflection and the non-diagonal are transmission coefficients.

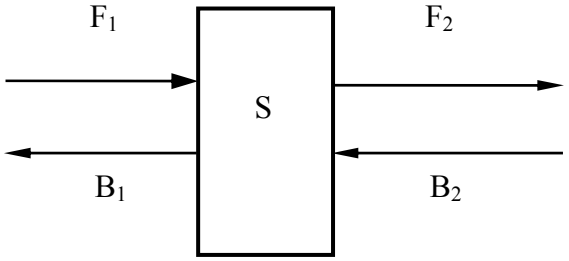

Figure. 7. Scattering matrix notations.

The incident and scattered wave amplitudes are connected as follows (fig.7):

$$\begin{pmatrix} \vec{B}_1 \\ \vec{F}_2 \end{pmatrix} = \begin{pmatrix} \hat{S}_{11} & \hat{S}_{12} \\ \hat{S}_{21} & \hat{S}_{22} \end{pmatrix} \begin{pmatrix} \vec{F}_1 \\ \vec{B}_2 \end{pmatrix} \tag{1}$$

The scattering matrix for the whole system is obtained by consequent cascading of elementary scattering matrices (Fig. 8):

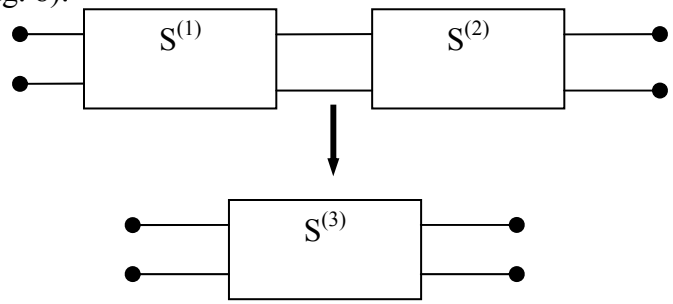

Figure. 8. Scattering matrixes $S^{(1)}$ and $S^{(2)}$ cascaded to the $S^{(3)}$ matrix.

where

$$S_{11}^{(3)} = S_{11}^{(1)} + \frac{S_{12}^{(1)} S_{11}^{(2)} S_{21}^{(1)}}{(1 - S_{11}^{(2)} S_{22}^{(1)})},$$

$$S_{12}^{(3)} = \frac{S_{12}^{(1)} S_{12}^{(2)}}{(1 - S_{11}^{(2)} S_{22}^{(1)})},$$

$$S_{21}^{(3)} = \frac{S_{21}^{(2)} S_{21}^{(1)}}{(1 - S_{11}^{(2)} S_{22}^{(1)})}, \tag{2}$$

$$S_{22}^{(3)} = S_{22}^{(2)} + \frac{S_{21}^{(2)} S_{22}^{(1)} S_{12}^{(2)}}{(1 - S_{11}^{(2)} S_{22}^{(1)})}.$$

If the electromagnetic fields of the waves are normalized like

$$E = \frac{1}{\sqrt[4]{\varepsilon}}(F + B),$$
$$H = \sqrt[4]{\varepsilon}\,(F - B), \tag{3}$$

then the reflection and transmission coefficients at the dielectric boundary are written as

$$R = \frac{1 - \sqrt{\varepsilon}}{1 + \sqrt{\varepsilon}}, \quad T = \frac{2\sqrt[4]{\varepsilon}}{1 + \sqrt{\varepsilon}}, \tag{4}$$

and the power conservation law is observed,

$$|R|^2 + |T|^2 = 1. \tag{5}$$

The scattering matrices for the dielectric boundary are:

$$S_3 = \begin{pmatrix} -R & T \\ T & R \end{pmatrix}, \qquad S_5 = S_3^T = \begin{pmatrix} R & T \\ T & -R \end{pmatrix}. \tag{6}$$

The scattering matrices S_1 and S_7 for the reflectors

$$S_1 = S_7 = \begin{pmatrix} -r & it \\ it & -r \end{pmatrix} \tag{7}$$

are chosen to provide zero reflection of two-reflector combination – dielectric boundaries (3 or 5) and supplementary reflectors (1 or 7) correspondingly.

The scattering matrices for the uniform sections

$$S_2 = \begin{pmatrix} 0 & \Lambda_1 \\ \Lambda_1 & 0 \end{pmatrix}, \qquad S_4 = \begin{pmatrix} 0 & \Lambda_d \\ \Lambda_d & 0 \end{pmatrix}, \qquad S_6 = \begin{pmatrix} 0 & \Lambda_2 \\ \Lambda_2 & 0 \end{pmatrix} \tag{8}$$

do not contain diagonal elements, and non-diagonal elements $\Lambda_{1,2} = \exp(ikL_{1,2})$, $\Lambda_d = \exp(ik\sqrt{\varepsilon}L_d)$, correspond to the phase shifts for section lengths.

The results of calculations for the described model with a of frequency 34.272 GHz, L_1=L_2=110 mm ε=9.8, r=0.5, t=$\sqrt{0.75}$ are presented below. The distances and dielectric permittivity correspond to the real window design shown in the next sections. The reflection

coefficients of both reflectors are equal to the reflection at the boundary of dielectric. This allows to realize the effect of resonant enlightenment known from a Fabri-Perrot interferometer with equal semi-reflecting mirrors. An elementary interferometer here is formed by the reflector and the boundary of dielectric. At certain frequency it has 100% transmission. So at any thickness of dielectric plate the system of two equal elementary interferometers can provide full resonant transmission (below called A-type resonance).

On the other hand these two elementary interferometers and dielectric-filled space in between form an interferometer of the next order, which can also provide resonant enlightenment (below called B-type resonance). So at the window system frequency characteristic (Fig.9) two resonances are observed. As it follows from the graph, the position of the B-type resonance depends on the dielectric plate thickness L_d unlike the A-type resonance. So due to B-type resonance the transmission bandwidth may be regulated by changing length L_d. Changing this parameter the reflection maximum between A- and B-resonances also changes. The transmission band is defined by a certain level of reflection (in Fig. 9 it is assumed as 0.01). At certain length L_d the pike goes above this level, so the defined transmission bandwidth changes stepwise by two or more times.

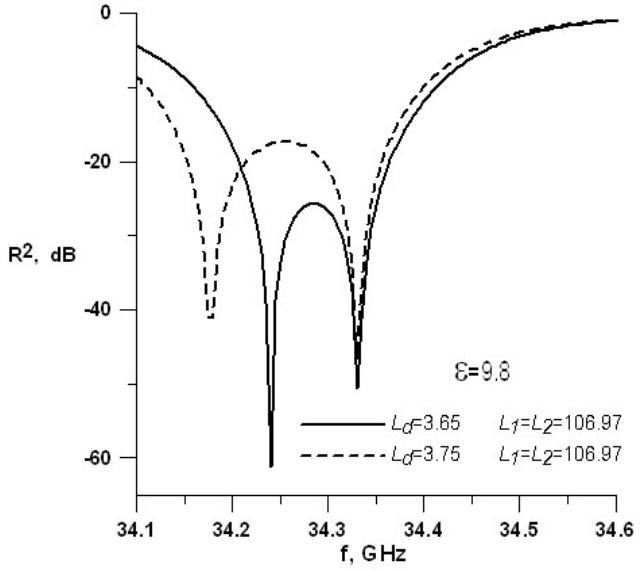

Figure 9. Typical view of frequency characteristics
for different slab thickness L_d.

Changing shoulders length L (for equal shoulders $L=L_1=L_2$) results in transmission band shift while the bandwidth stays the same (Fig. 10)

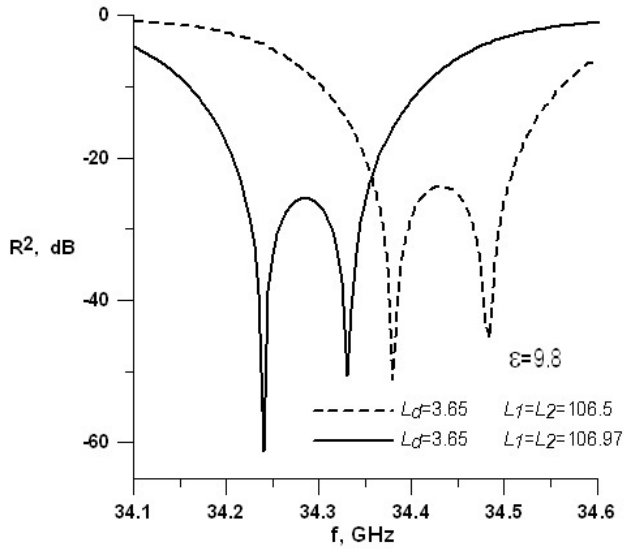

Figure 10. Typical view of frequency characteristics for various length $L = L_1 = L_2$.

The longitudinal field distributions at different points of transmission band are shown in Fig.12. As follows from the graph the A-type resonance provides the lowest electric field at the dielectric surface and inside. As the position of the A-resonance does not depend on L_d, this level (below called E_0) also stay constant for all characteristics at any L_d . The highest surface field level within the transmission band (below called E_1) is observed at the frequency margins, and $E = E_1 / E_0$ is the critical parameter to be decreased in order to prevent the surface breakdown. This parameter squared and inverted is plotted at Fig. 11 versus L_d. Like the transmission bandwidth it is step-wise changed by the reason mentioned above.

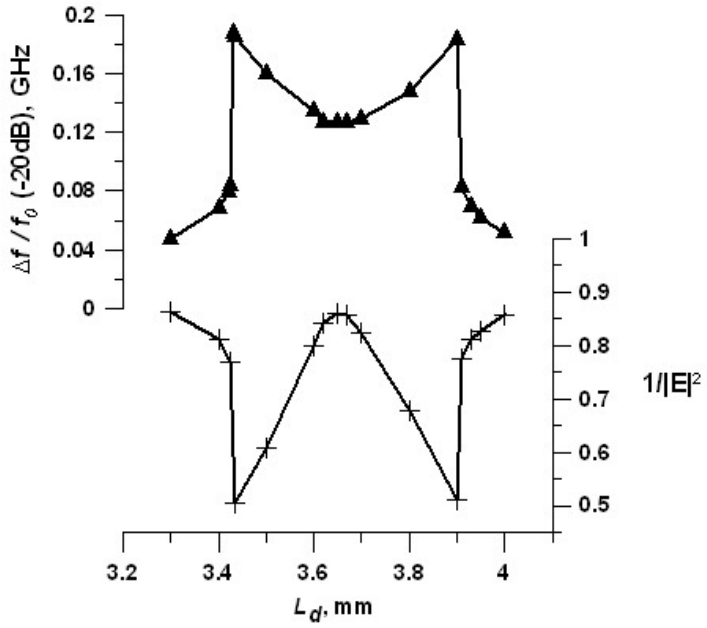

Figure 11. Operating frequency band (reflection below -20dB) and normalized maximum field on the dielectric surface versus slab thickness L_d.

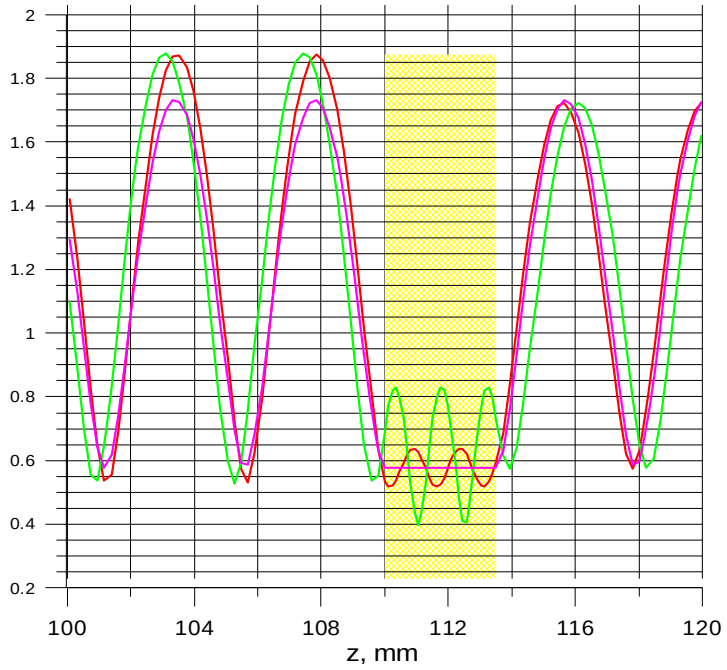

Figure 12. Longitudinal distributions of electric field near the window disc (marked by yellow color). Pink curve with constant electric field inside the dielectric corresponds to ideally matched dielectric surface (resonance A). Two other curves (red and green) with the field oscillating inside dielectric correspond to near- and far- borders from the resonance A of the -20dB frequency band.

Fig. 13 illustrates the influence of shoulders mismatch on the frequency characteristic of the model. It is shown that the mismatch parameter $\Delta = (L_2 - L_1)/L_1$ must not be more than 0.05 for total window reflection $|R|^2 < 0.01$.

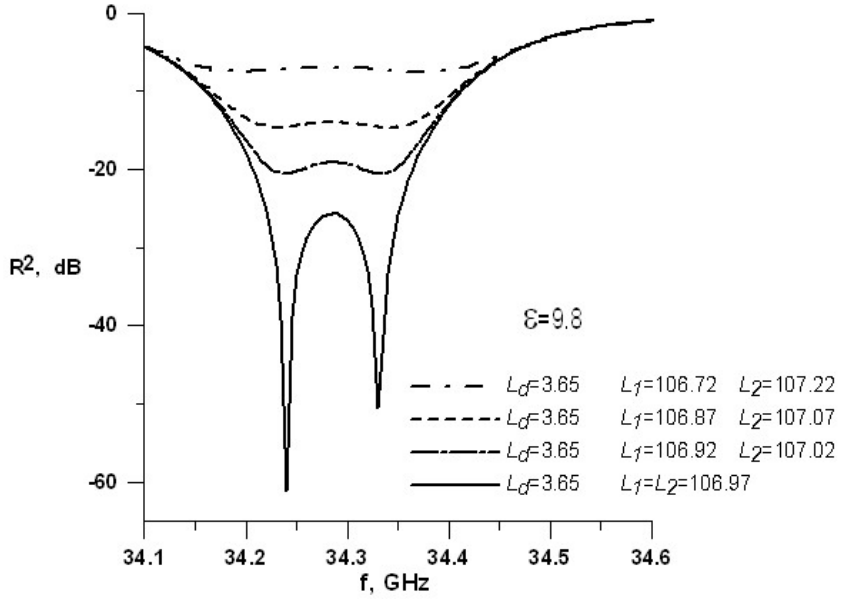

Figure 13. Frequency characteristics at different mismatch of shoulders.

IVb.2. Design of the window mock-up

The critical point of the design stage is a selection of the window diameter. The computer simulation of the flattened field distribution in the alumina ceramics window with operating diameter 40mm predicts a 5.5 kV/mm peak value of electric field sufficient for 100 MW power transmissions. 60 mm diameter window is capable to transmit 200 MW power. Below the window mock-up with 40 mm disc is discussed.

Simplified plane wave analysis gave us preliminary estimations for the window parameters and geometry. Step-by-step TW window optimization was carried out for reflector and up-taper profiles, frequency adjustment unit and ceramics disk thickness in accordance with general design principles described in previous sections. Schematic of the window block depicted in Fig. 14. The left half of the system is identical to the right one, so only half of the TW window is shown in the figure.

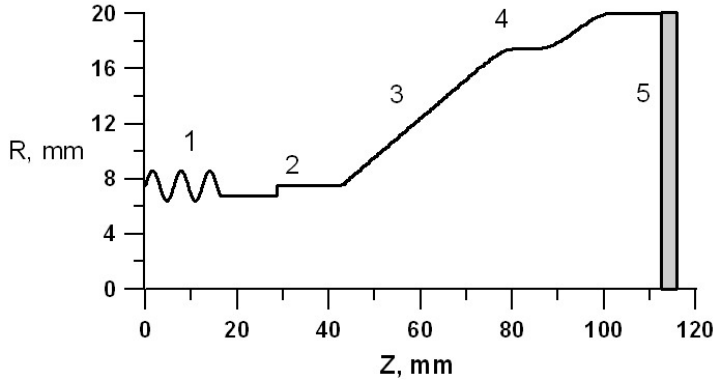

1 – TE_{01} Bragg reflector ∅15 mm,
2 – Section with variable length ,
3 – Cone ∅15 ⇒ ∅32,
4 – Synthesized up-taper ∅32⇒ ∅40,
5 – Ceramics disc ∅40mm.

Figure 14. One half of the window block with the mode converters and the reflector.

The enumerated components in Fig.14 are the following:

1. The TE_{01} mode reflectors are performed with sinusoidal corrugations. Sinusoidal Bragg reflector provides reflection level of $|r|^2$=0.26 for the incoming TE_{01} mode. Scattering matrix technique was used for calculation of the reflector and choosing amplitude and period of corrugations. In this design the input diameter of the reflector was 15mm.
2. A uniform guide section with variable length follows the Bragg reflector, in order to provide fine frequency tuning.
3. Simple up-tapering cone section matches frequency adjusting section and following synthesized converter.
4. Synthesized cone section provides special mode conversion and up-tapering to the window disk diameter (40mm). The optimal symmetrical mode mixture with intensity flattening (Fig. 15) is formed at the operating frequency. Mutual phases of the propagating modes equal zero or π at the central window plane, so two identical sections were used. Up-taper profile synthesized by means of algorithm described in [15]. Field intensity distribution at the window has a 1.4 times lower maximal value in comparison with pure TE_{01} mode.
5. Alumina ceramics disk (BK 100-1) was incorporated in the centre of symmetrically placed shoulders of the mock-up. Disk thickness was selected 3.6 ± 0.01 mm, in

accordance with measured dielectric permittivity value ε = 9.5. Besides, loss tangent is less than $2 \cdot 10^{-4}$ was assumed.

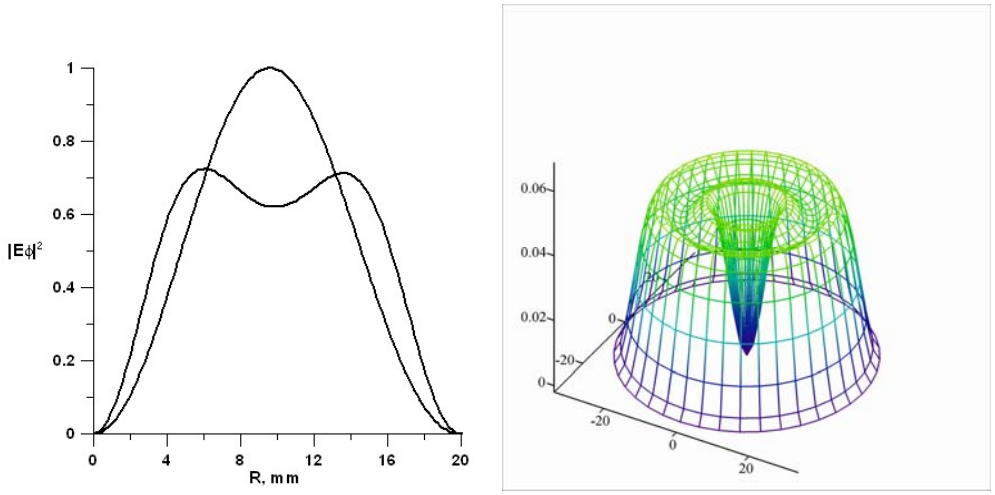

Figure 15. Intensity of electric field on the window surface for the optimized TE_{01}-TE_{02}-TE_{03} mode mixture and pure TE_{01} mode. The ratio of the maximum intensities is 1.4:1. 3-D view of the field intensity on the surface is shown on the right picture.

Calculated power transmission coefficient (including ohmic losses) for the window mock-up (Aluminum tapers and ceramics with loss tangent $2 \cdot 10^{-4}$) exceeds 99.2% at 34.272GHz (Fig. 16).

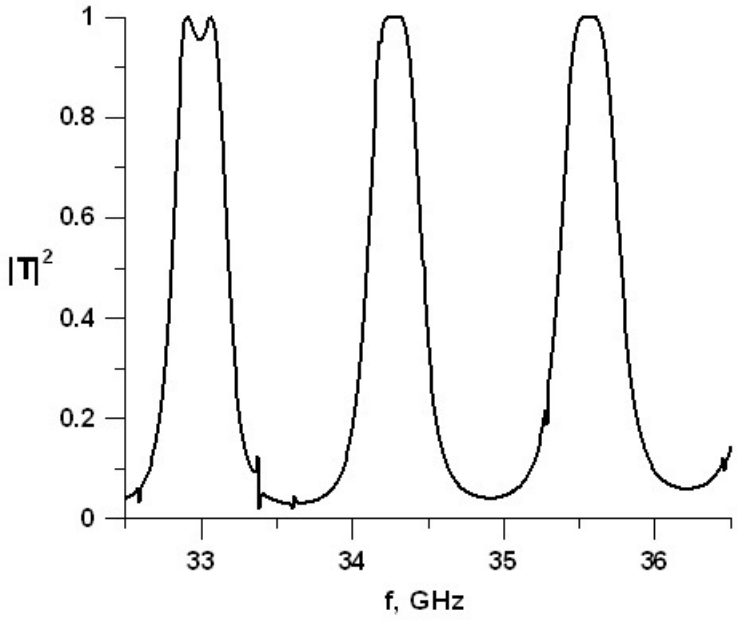

Figure 16. TW window mock-up power transmission.

Field distribution in the waveguide (at $R = R_W/2$) along the window mock-up at the central frequency 34.272 GHz is shown in Fig.15. Minimal electric field value 5.5 kV/mm for 100 MW power level corresponds to the ceramics disk position ($z \approx 100$ mm). A TW window with disc diameter 63.5mm provides a 200 MW power transmission respectively.

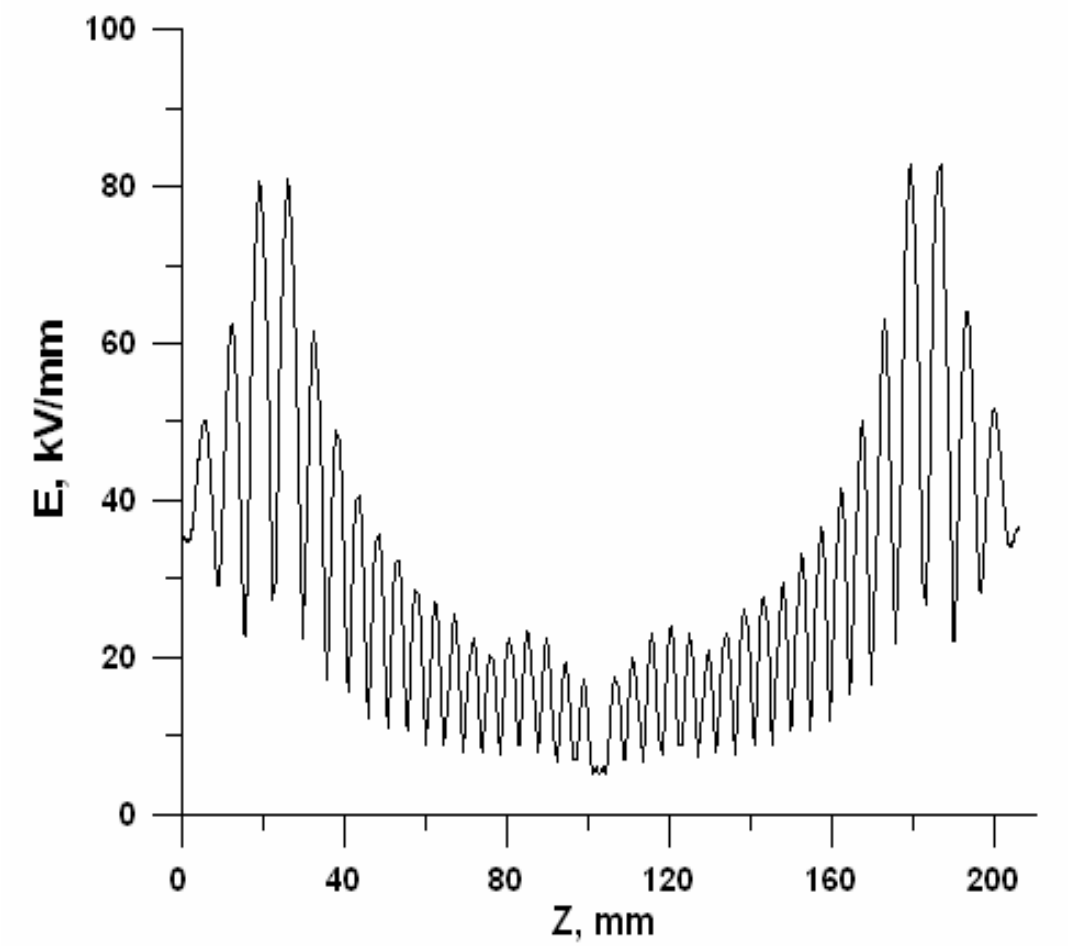

Figure 17. Calculated electric field amplitude distribution in the window-mock-up at 34.272 GHz

.

IVb.3. Low-power test results for the window mock-up

The window mock-up (Fig.18) was designed, manufactured and tested at low power level (20mW).

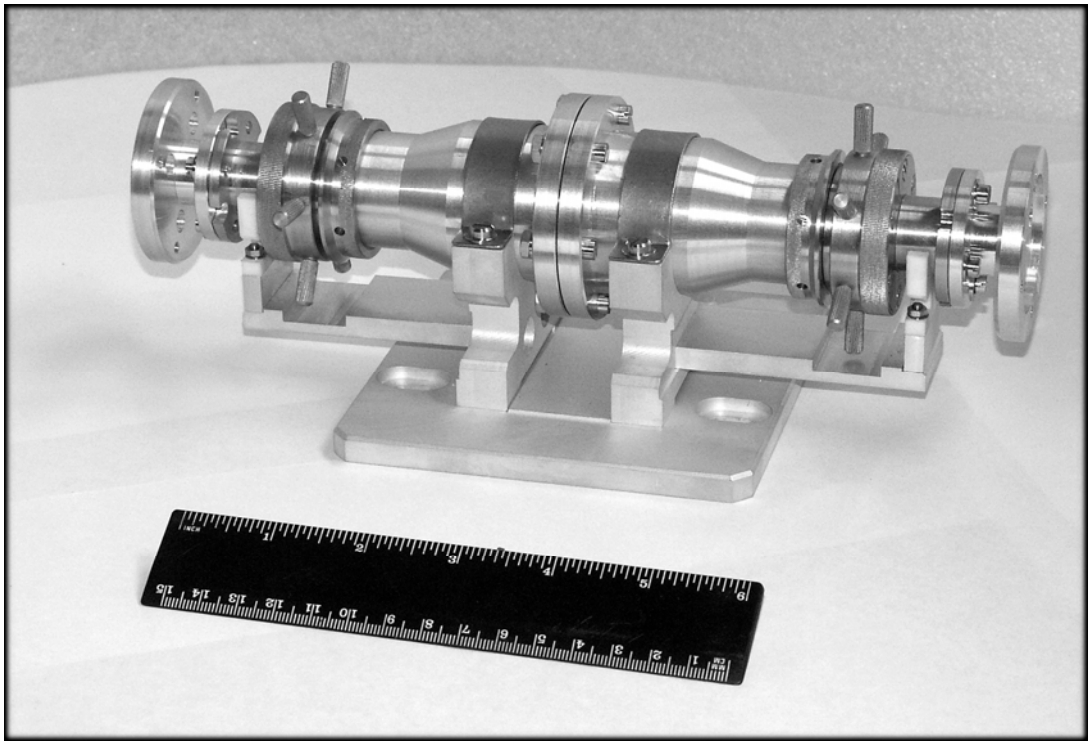

Figure 18. Photograph of the low-power window mock-up.

Experimental set-up scheme is shown in Fig.19.

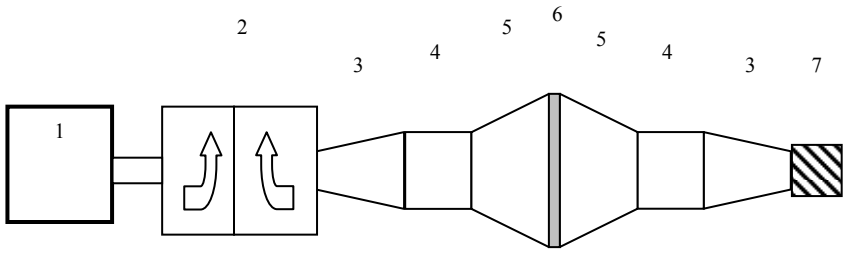

1 – BWO 26 GHz - 37 GHz; 5 – synthesized window tapers, 2 – directional couplers with detectors, 6 - window disk ∅40 mm, 3 – Marie mode transducer, 7 – matched load, 4 – TE_{01} mode reflector

Figure 19. Scheme of the set-up for reflection coefficient measurements.

Polycrystalline alumina ceramics (BK100-1) disk was used for TW window tests. For this ceramics the tangent losses approximately $2 \cdot 10^{-4}$ was measured. Additional component, Marie mode transducer, with output internal diameter of 11.4 mm was used for mock-up excitation. It transforms fundamental TE_{10} mode of rectangular wave guide into the symmetrical TE_{01} mode of circular one. Output TE_{01} mode purity exceeds 99% at the operating frequency 34.272 GHz.

According to the analysis, equal lengths of the window shoulders diminished reflection coefficient in a best way for our purposes. As follows from the graph (Fig. 20), measured reflection coefficient of less than -25 dB was achieved in the frequency band ~100 MHz. This level of reflection is defined by parasitic reflections in the measurement duct. The picture show that calculated and measured window parameters agree well. In Fig. 21 measured transmission coefficient is show.

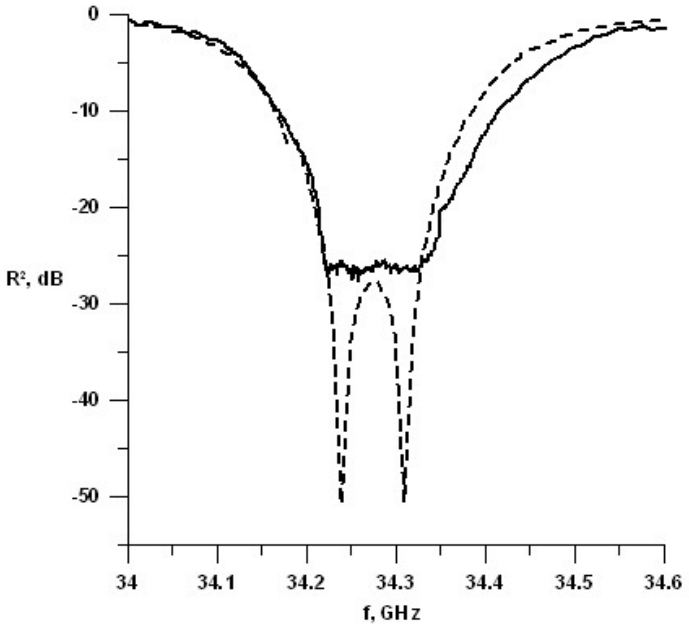

Figure 20. Calculated and measured reflection coefficient characteristics. Ceramics is BK 100-1. Disk thickness 3.6 ± 0.01 mm, ε = 9.5, loss tangent $2 \cdot 10^{-4}$.
Solid line – measured, dashed line – calculated.

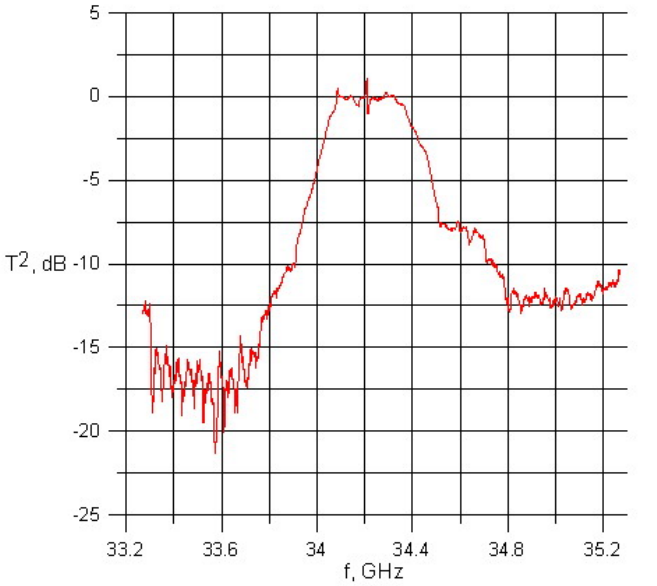

Figure 21. Measured transmission coefficient characteristics.

IVc. Modification of the resonant ring

A Ka-band resonant ring using a traveling TE_{01} wave in cylindrical waveguide has had preliminary design, fabrication, and low-power tests by Omega-P, under DoE-sponsored SBIR Phase I grant DE-FG02-03ER 83737, entitled *Ka-band resonant ring for high-power testing,* that ran between 07/21/03 and 04/20/04 Low power measurements have already shown a maximum effective power gain that exceeded 35:1 at the design frequency of 34.272 GHz. Estimated round trip losses in the ring are very low - approximately 3% - including Ohmic losses and losses due to scattering of the operating mode TE_{01} into other modes [15]. However, improvements can be incorporated to decrease the losses in the ring, and thus to increase the effective power gain and utility for testing other low-insertion-loss components.

The most critical component which defines mainly the losses in the ring is a TE01 miter bend. There are four bends in the ring and losses in one bend should be multiplied by 4. It also should be noted that the component is very important since it is used in accelerator transmission lines and delay lines. Now in our work during Phase I we have shown that the losses in the bend can brought down from the value 0.7-0.8% to 0.3-0.4%. The resonant increase of power traveling in the ring can be enhanced practically two times. Let us consider below the idea of improvements.

IVc.1. Low-loss miter bend for H_{01} transmission line

Our approach to the losses minimization consists of two steps. The first step includes a choice and a calculation of corresponding eigenmodes in an auxiliary virtual quasi-optical resonator which is formed by two mirrors whose apertures coincides to the waveguide apertures in the gap and the distance between mirrors corresponds to the gap length (Fig. 22). A miter bend with a flat mirror can be considered to have the same auxiliary resonator (Fig. 23). For a miter bend with a phase correcting mirror one should consider a cavity with a phase corrector between

the mirrors. Shapes of the cavity mirrors are subject of choice taking into account additional requirements and restrictions. Note that a confocal cavity has the minimal diffraction losses [e.g. 11-13], however its choice is not optimal in some practical cases (see the later comments).

When the cavity is defined then it is necessary to calculate eigenmodes with a required symmetry. For example, if one consider HE_{11} mode propagation in axis-symmetrical waveguides then it is necessary to calculate the first scalar mode close to Gaussian wave beam (0 order scalar mode symmetry).

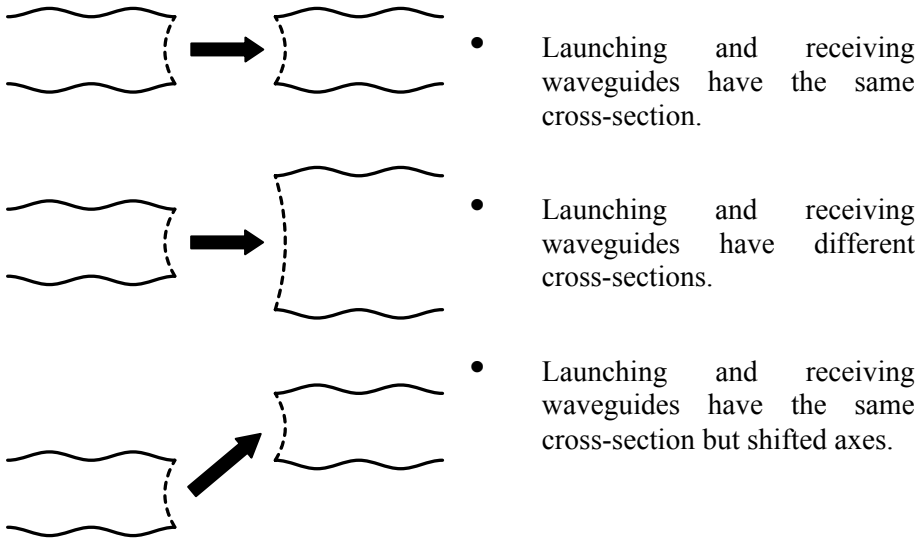

Figure 22. Different versions of auxiliary cavities interesting for practice.

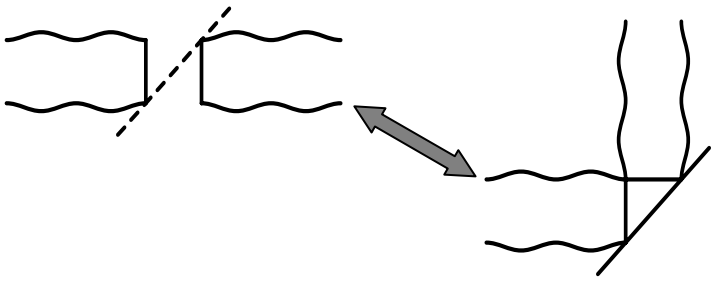

Figure 23. Waveguide gap and corresponding miter band with a flat mirror.

It is optimal to use the direct iteration method [12] which simulates the wave beam propagation from mirror to mirror and allows to get a consecutive number of modes sorted in the order of loss increasing. Algorithms of modal synthesis and their calculation are also described in [14]. Having calculated the mode spatial structure and losses it is necessary to represent this mode as a sum of waveguide modes with definite amplitudes and phases. The second step on the way of the loss minimization is a mode converter synthesis basing on a new method described in [15]. Converter's profile depends on the chosen auxiliary resonator parameters (i.e., focal lengths of the mirrors), so in many cases minimal diffraction losses of confocal resonator are negated by greater losses in the corresponding converter.

It is clear that by following this way the diffraction losses in waveguide gaps can be minimized. According to our calculations (see also the next section) the solutions obtained show much less losses than the components known before.

The designed low-loss miter bend consists of two specially shaped waveguide tapers and a flat mirror. Each taper has length L=250 mm, input and output cross-section's diameters are D_1=40 mm and D_2=63.5 mm, and the distance between the taper's output cross-section and the center of the mirror is d=34 mm. To minimize diffraction losses, we synthesize the second low-loss eigenmode of the cavity formed with two virtual focusing mirrors positioned at the tapers' cross-sections and the miter bend mirror using the method described in [16]. The second eigenmode is chosen because its symmetry is the same as the main H_{01} mode of the transmission line. This field distribution, once obtained at the first taper's output, decreases the amount of diffraction losses in the gap to less than 0.3%. The first taper is used to convert input H_{01} to the mixture of H_{0n} modes which represents the field distribution of the cavity eigenmode. The taper's profile was synthesized using a special technique described in [17]. Due to the symmetry, after passing the gap only field's phase sign is changed in comparison to first taper's output cross-section (Fig. 24). Therefore, to convert radiation back to H_{01} mode we can use the second taper's profile identical to the reversed one of the first taper (Fig. 25).

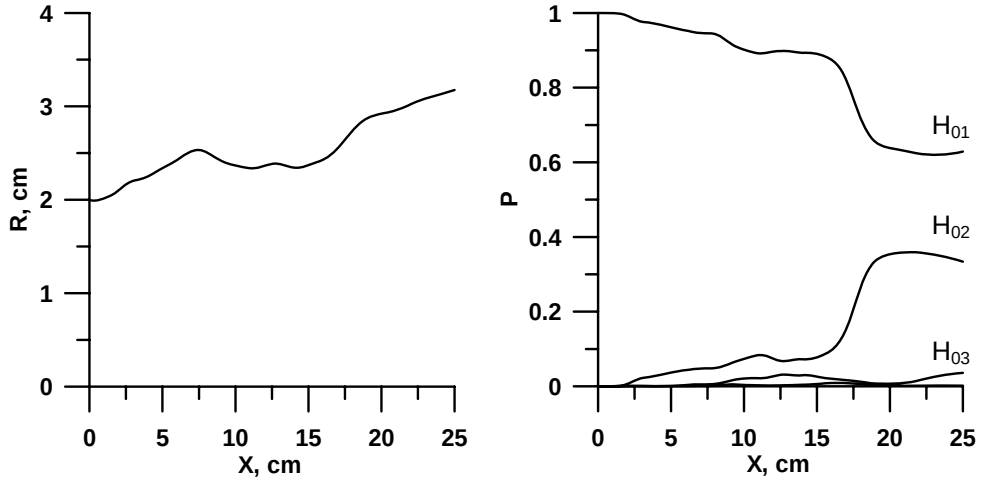

Figure 24. Left part – first taper's profile, right part – wave powers inside the taper

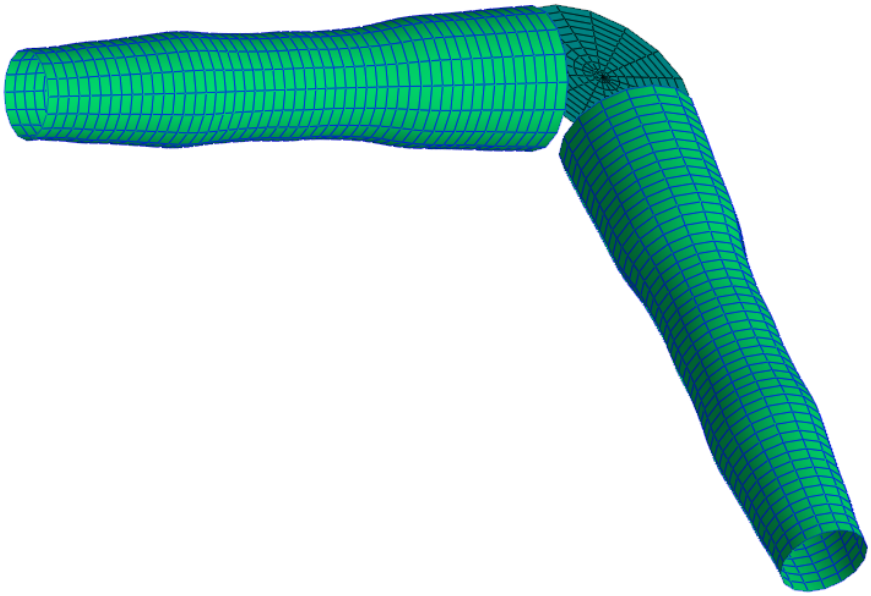

Figure 25. 3D-view of the miter bend internal surfaces – two tapers and flat mirror.

V. CONCLUSIONS

A multi-mode traveling wave type window was studied using a simple plane-wave model and based on an accurate multi-mode numerical code. This study gave clear understanding of the main window issues: requirements to the dielectric plate and reflectors, tolerances to the window parts, electric fields in critical areas, reflection and transmission characteristics, frequency band. A Ka-band traveling wave window in an oversized waveguide was designed for high-power transmission. Symmetric TE_{on} modes having low ohmic losses and zero electric field at the guide wall were used as the operating ones. Special converters were placed symmetrically to the alumina ceramics disk. Special attention was paid for choice of the disk thickness for appropriate transmission frequency band width. Central frequency tuning can be provided by the simultaneous length adjustment of both converters. The computer simulation of the field distribution in the window with operating diameter 40 mm predicts a 5.5 kV/mm peak value of electric field on the disc surface sufficiently low for 100 MW power transmission at frequencies in Ka-band. A 60 mm diameter window is capable of safely transmitting 200 MW power.

A 40 mm diameter window mock-up was built and tested at a low-power level. Operating frequency band for Al_2O_3 ceramic disk is approximately 100 MHz at -26 dB power reflection and >99% transmission level. All measured window characteristics measured agreed well with the design parameters. The main technological questions of the window fabrication were studied: methods of Alumina ceramic disc cutting, polishing and high-temperature brazing was developed at IAP/Omega-P. Technology of manufacturing of synthesized complex-shape waveguide tapers for the window and miter bends was also developed.

Having done these studies we can conclude that conceptual design work carried out by Omega-P during Phase I has met all objectives of the project, and that engineering design and fabrication of the high-power vacuum window and its testing with the resonant ring can begin.

VI. REFERENCES

[1] O.A. Nezhevenko, V.P. Yakovlev, M.A. LaPointe, E.V. Kozyrev, S.V. Shchelkunov, and J.L. Hirshfield, "Status Of 34 GHz, 45 MW Pulsed Magnicon," PAC2005, Knoxville, May 16-20, 2005, p. 1922-1924.

[2] R.W. Assmann, F. Becker, R. Bossart, *et al*, "A 3 TeV e^+e^- Linear Collider Based On CLIC Technology," CERN 2000-008, 28 July 2000.

[3] E. Jensen, "30 GHz Stand-Alone Power Source For Development of CLIC RF Equipment," CLIC Collaboration Meeting, 19 May 2004 (see also http://clic-collaboration-meeting.web.cern.ch/clic-collaboration-meeting/presentations/WP9%20 Erk.ppt)

[4] A. Bogdashov, G. Denisov, D. Lukovnikov, Y. Rodin and J. Hirshfield. "Ka-Band Resonant Ring for Testing Components for a High-Gradient Linear Accelerator". *IEEE Transactions on Microwave Theory and Techniques*, Vol. 53, No. 10, October 2005, pp. 3152-3154.

[5] H. Matsumoto, "Development of a high power RF-window at S-band", Int. Accelerator School in Japan, 1996.

[6] Y. Saito, N. Matuda, S. Anami, H. Baba, A. Kinbara, G. Horikoshi, J. Tanaka, "Breakdown of alumina RF windows", *IEEE Trans. Electr. Insul.*, Vol. 24, pp. 1029-1032, 1989.

[7] S. Yamaguchi, Y. Saito, S. Anami, S. Michizono. "Trajectory Simulation of Multipactoring Electrons in an S-band Pillbox RF Window", *IEEE Trans. on Nuclear Science*, 1992, V.39, No.2, pp.278-282.

[8] International Study Group Progress Report on Linear Collider Development, *SLAC-Report-559, KEK Report 2000-7*, April 2000, pp.168-172.

[9] A. Neuber, J. Dickens, D. Hemment, H. Krompolz, L.L. Hatfield, M. Kristiansen. "Window Breakdown Caused by High-Power Microwaves", *IEEE transaction on Plasma Science*, 1998, V.26, No.3, pp.296-303.

[10] A. Valfells, L.K. Ang, Y.Y. Lau, R.M. Gilgenbach. "Effects of an external magnetic field, and of oblique radio-frequency electric fields on multipactor discharge on a dielectric", *Physics of Plasmas*. Vol.7, No.2, Feb. 2000, pp.750-757.

[11] W.R. Fowkes, R.S. Callin, E.N. Jongewaard, D.W. Sprehn, S.G. Tantawi, A.E. Vlieks, "Recent advances in high power RF windows at X-band", *AIP Conference Proc*.474: pp.289-295, 1999.

[12] J. Nielson, L. Ives, S.G. Tantawi, "Design and test of a 100 MW X-band TE01 Window" *IVEC 2002 Conference Proc*., pp.218-219.

[13] S.Yu. Kazakov, "A new traveling-wave mixed-mode RF window with low electric field in ceramic-metal brazing area", *KEK preprint*, Aug. 1998, pp.98-140.

[14] S.Yu. Kazakov, "RF window with TW in ceramics", *Int. Workshop on Pulsed RF power Sources for linear colliders* (RF93), July 5-9, 1993, Dubna-Protvino, Russia.

[15] G.G. Denisov, G.I. Kalynova, D.I. Sobolev. "Method for synthesis of waveguide mode converters". *Journal of Radiophysics and Quantum Electronics*, 2004, V.47, issue 8, pp.615-620.

[16] J.M. Nelson, P.E. Latham, M. Caplan and W.G. Lawson. "Determination of the resonant frequencies in a complex cavity using the scattering matrix formulation", *IEEE Trans. Microwave Theory Tech.*, Vol.37, No.8, 1989.

[17] V. I. Belousov, G. G. Denisov, A. V. Chirkov, *Methods of calculation and parameter control of the eigenmodes of a simple two-mirror cavity*, Journal of Radiophysics and Quantum Electronics, V.43, issue 8, 2000, pp. 663-670.

[18] J.L. Hirshfield, O.A. Nezhevenko, M.A. LaPointe, V.P. Yakovlev, "Technology Developments for a Future Millimeter-Wave High-Gradient Linear Accelerator", *2004 Joint Int. Conf. on Infrared and MM Waves*, Conference Digest, pp.529-530.